Impact of the Left Atrium Morphology on Hemodynamics in Atrial Fibrillation: A Computational Fluid Dynamics Study

João Lameu[1], João G B Torro[1] and Rodrigo L Amaral[1]

[1]Federal University of ABC, São Bernardo do Campo, Brazil

Abstract

Atrial Fibrillation (AF) elevates thromboembolic risk, with the Left Atrial Appendage (LAA) morphology playing a pivotal role. The LAA is the primary site of thrombus formation in AF patients. While LAA morphological classification has traditionally been subjective, recent studies advocate for quantitative parameters (volume, depth, ostium area) to enable objective risk assessment. This study investigated how LAA and left atrial (LA) morphology affect hemodynamics and thromboembolic risk in AF patients by performing 3D hemodynamics in five patient-specific LA models with distinct morphological features. Enlarged atria and deeper LAA exhibited higher thrombotic risk due to low Time-Averaged Wall Shear stress and elevated Oscillatory Shear Index and Relative Residence Time. Also, pulmonary veins alignment and cross-sectional area affected the global hemodynamics. Asymmetric LAA morphologies caused higher flow disturbance, while simpler shapes showed lower thrombogenic potential. The results highlight the importance of personalized hemodynamic analysis to guide interventions and stratify high-risk patients, improving clinical outcomes. 3D hemodynamic models, aligned with the digital twin concept, emerge as innovative tools in precision cardiology, integrating anatomy and hemodynamics to predict AF-related complications.

1. Introduction

Atrial fibrillation (AF) is a cardiac arrhythmia characterized by disorganized impulses in the atrial muscle, resulting in deprecated atrial pumping and about of 20% to 30% reduction in ventricular pumping efficiency. Although more common in elderly individuals, between 75 and 80 years old, it can also affect younger people. AF is a chronic condition, with a prevalence of 2.9% associated with increased morbidity and mortality [1]. The risk of thromboembolic events in AF patients is related to the morphology of the left atrial appendage (LAA) [2]. There are different types of LAA morphology, such as windsock, chicken wing, cactus, and cauliflower, that impacts the hemodynamic behavior. The chicken wing morphology, the most common [3,4], presents lower risks of thrombosis due to fewer blood stagnation zones [3]. However, some researchers point out that morphological classification can be subjective [6,7], and it is preferable to use more objective parameters, such as the area, depth and LAA volume [8,9].

The hemodynamic characteristics during AF is essential for improving patient care, optimizing treatments, and increasing the healthcare system efficiency. Computational Fluid Dynamics (CFD) is a valuable tool in this context, as it allows detailed flow field analysis, including estimation of hemodynamic indicators based on wall shear stress, related to inflammatory and remodeling processes of cardiovascular system. This study leverages patient-specific computational fluid dynamics (CFD) to elucidate how left atrial (LA) and appendage (LAA) morphometrics—including volume, pulmonary vein (PV) alignment, and cross-sectional areas—synergistically dictate 3D hemodynamic dysfunction and thromboembolic risk in AF. By integrating quantitative anatomy with high-fidelity flow simulations, we expect that our findings advance precision cardiology by shifting from subjective shape classification to physics-based risk stratification, laying the groundwork for digital twin applications in stroke prevention.

2. Materials and Methods

Five patient-specific models of LA (Fig. 1) were obtained from a public database [10]. Table 1 presents the morphometric data of the five evaluated LA. The analysis of Table 1 reveals that the LA(05) anatomy showed higher level of remodeling and enlargement, in contrast with the LA(01), which has a smaller volume. In general, the average LA volume in healthy individuals is about 73 mL, while in patients with AF it is greater than 130 mL [17]. The LA(03) anatomy stands out due to the larger LAA volume, being two to three times greater than the others. However, several mechanical and geometric factors influence atrial hemodynamics and the thromboembolic risk of each patient, making a detailed analysis of velocity and hemodynamic indicators necessary [18]. The 3D geometries were used to generate hybrid meshes with about 1.8 million elements. In wall-zones, 10 inflation layers were used (first layer thickness of 0.01 mm, growth rate of 1.2) for accurate velocity gradient estimations.

The main characteristics of the model are: laminar, isothermal, incompressible, transient/pulsatile flow, with non-Newtonian blood behavior (Carreau-Yasuda model) [11].

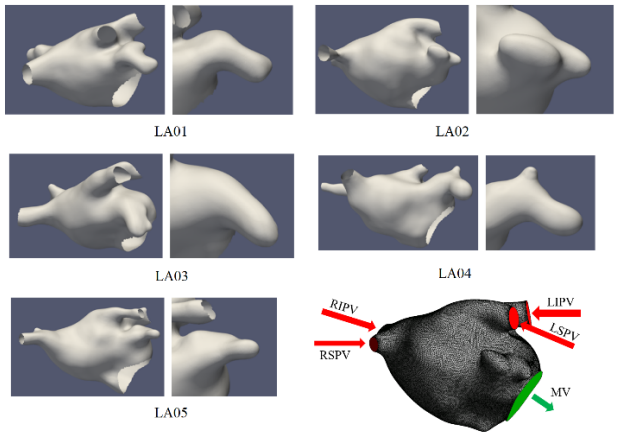


Figure 1. Patient-specific LA geometries (LA01 to LA05) from open dataset [10], with LAA details and example of numerical mesh with boundary conditions (pulmonary veins (PV): right inferior (RIPV), right superior (RSPV), left inferior (LIPV), left superior (LSPV), mitral valve (MV)).

Table 1. Morphometric data of the patient-specific LA.

LA	(01)	(02)	(03)	(04)	(05)
LAA morphology*	CW	CC	CF	WS	CW
LA volume (cm³)	101	135	143	143	174
LAA volume (cm³)	4.5	3.0	9.0	2.9	3.6
LAA ostium area (cm²)	3.9	4.4	5.0	3.4	3.4
LAA depth (cm)	1.1	0.7	1.8	0.8	1.0
LSPV area (cm²)	1.0	0.9	0.7	0.5	1.9
LIPV area (cm²)	0.8	1.5	0.5	1.7	1.6
RSPV area (cm²)	1.4	0.4	1.0	0.7	1.7
RIPV area (cm²)	0.8	1.3	0.4	0.3	1.6
MV area (cm²)	6.3	8.1	8.4	7.9	8.5

* Approximated (subjective) LAA morphology classification: CW – chicken-wing, CF – cauliflower, CC – cactus, WS – windsock.

The boundary conditions were: Inlets – pulsatile velocity, considering a systolic/diastolic relationship of 1.0, according to clinical findings [12]. Outlet: constant pressure of 8 mmHg at the mitral valve (MV), considering open with a fixed area along the cardiac cycle [13]. Walls: no-slip condition, due to the viscous blood, considering rigid-walls, the worst AF scenario (no atrial contraction).

The Ansys CFD package was used. For the numerical solution, the High-Resolution advection and the second-order Euler (Backward) schemes were employed. The residual target (RMS) of 1 x 10^{-4} was employed. For each case, 5 complete cardiac cycles were simulated, lasting 0.8 s, equivalent to a heart rate of 75 bpm, using a time step of 1 x 10^{-3} s, and time-averaged values were obtained for the last two cardiac cycles.

The thrombosis-prone regions were assessed by well-established hemodynamic indicators based on *WSS*: Time-Averaged Wall Shear Stress (*TAWSS*), Oscillatory Shear Index (*OSI*), that describes the temporal change in the *WSS* direction relative to the predominant flow, and Relative Residence Time (*RRT*), with the thromboembolic risk classification given according to Table 2 [14-16].

Table 2. Thromboembolic risk classification proposed based on literature data [14-16].

Indicator	Thrombogenic risk	
	Low	High
TAWSS	> 0.4 Pa	< 0.1 Pa
OSI	< 0.10	> 0.25
RRT	< 10 Pa^{-1}	> 25 Pa^{-1}

3. Results and Discussion

Figure 2 shows the results for the hemodynamic indicators *TAWSS*, *OSI* and *RRT* along the average blood velocity. Fig. 2(a) shows the 3D field (volume rendering) of the time-averaged velocity in LA, with the atrial anatomy displayed in translucent gray. In the 3D volume rendering, the transparent regions indicate areas of significant blood stasis (time-averaged velocities below 5 cm/s). It was observed that morphological variation directly affected the velocity behavior in the atrium as a whole, especially in the AAE, which was considered critical for thrombus formation in patients with AF [19].

Fig. 2(a) shows that the average velocity in the AAE region was somewhat similar in both LA(01) and LA(03), even though the AAE of LA(03) has approximately twice the volume and higher depth. This may be related to the shape of the appendages. LA(01) has a chicken-wing shape, while LA(03) has a cauliflower-like morphology with two lobes. It is important to note that even in the smaller lobe of this appendage, located in the middle portion, there were significant stasis zones, confirmed by the hemodynamic indicators (*TAWSS*, *OSI* and *RRT*). The LA(02) exhibited a distinctive flow behavior, with the second smallest atrial and AAE volume, along relative large areas of moderate *TAWSS (< 0.5 Pa)*, and low *TAWSS* (< 0.1 Pa) especially in the AAE lobes (Fig. 2b). This can be attributed due to the high-velocity of blood flow colliding with the posterior wall of the atrium and moving towards the mitral valve, avoiding the area near the AAE. The five patient-specific LA presented distinct morphological aspects, including, higher PV asymmetry (RSPV = 0.4 cm² vs. LIPV = 1.5 cm²) of LA(02), in contrast with more balanced PV areas (e.g., LA(01): LSPV = 1.0 cm², RIPV = 0.8 cm²) of LA(01) and LA(03). The asymmetric PVs of LA(02) caused flow collision near the posterior wall, diverting blood from the LAA, creating recirculation zones and explaining its low *TAWSS* in appendage zone, even with shallower LAA). LA(04) had the highest velocity in its atrial appendage, with the smallest volume, while LA(05) exhibited the lowest average velocity in the atrium, which was related to the largest atrial volume among the simulated cases.

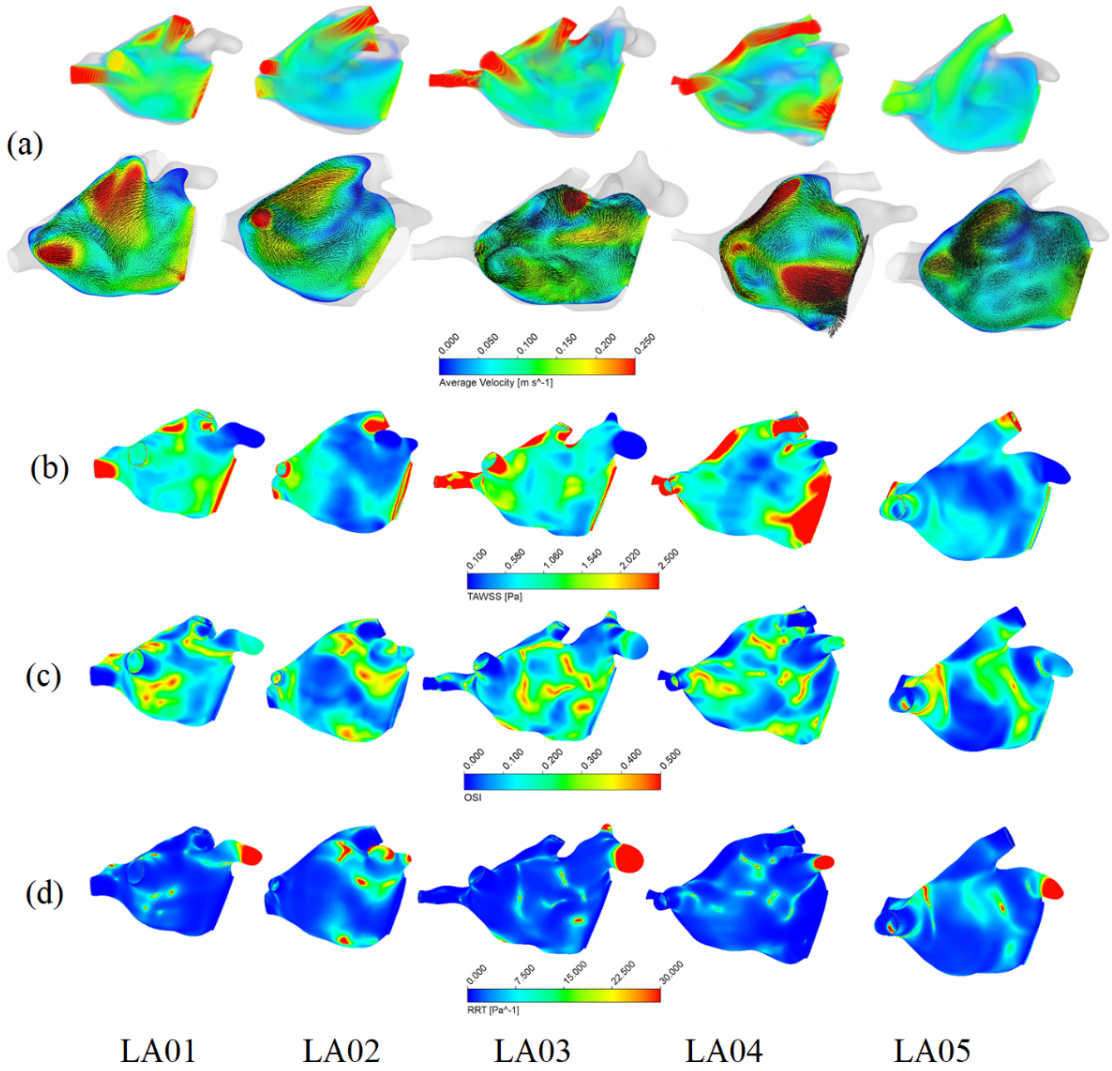


Figure 2. (a) 3D field of time-averaged velocity and respective mid-plane (located between PVs) vector fields, (b)-(d) hemodynamic indicators on LA/LAA surfaces: (b) *TAWSS*, (c) *OSI*, (d) *RRT*.

From Fig. 2b the LA(02) and LA(05) exhibited areas with low *TAWSS* (around 0.1 Pa), associated with critical limits for clot formation [20]. In the case of LA(02), this occurred due to the hemodynamic behavior, while LA(05), with a larger atrial volume, showed lower velocities and consequently lower shear stresses. LA(01), LA(02), and LA(04) exhibited *OSI* peaks at the LAA apex, in contrast to LA(03) to LA(05), which showed higher *OSI* regions in intermediate areas of the appendage (Fig. 2c). LA(02) also presented regions of higher recirculation at the LAA ostium, which are directly related to the hemodynamic patterns resulting from the orientations of the pulmonary veins [8]. It is worth noting that appendages with multiple lobes, such as LA(03), also showed *OSI* peaks in these locals [21] (Fig. 2c).

The *RRT* complemented the thromboembolic risk analysis, highlighting the most thrombogenic prone areas (Fig. 2d). These regions included the LAA apex, consistent with clinical findings [19] and in silico hemodynamics studies [4,8]. The regions with the highest thromboembolic potential (low *TAWSS* combined with high *OSI* and *RRT*) corresponded to an increase in the blood stasis, associated with lower shear deformation rates [4].

Analyzing the morphology of the appendage, it became clear that the shallower the AAE depth, the lower the risk of thrombus formation, as highlighted by the hemodynamic indicators of LA(02) and LA(04), compared to the other left atria, especially LA(03), which has a deeper and larger atrial appendage volume.

4. Conclusions

This study analyzed the hemodynamic behavior of five models of patient-specific left atrium anatomies, revealing

significant variations in blood flow and thromboembolic risk. The results indicated that atrial volume, appendage shape, and pulmonary vein alignment directly influenced the hemodynamic patterns and the risk of clot formation. The LA(02) and LA(03) atria, with lower *TAWSS* and significant blood stasis areas, showed a higher propensity for thromboembolic events, as confirmed by the *OSI*, *RRT*, and *ECAP* indicators. The atria with more uniform blood flow patterns, such as LA(01) and LA(03), showed lower thromboembolic risk, likely due to the more symmetrical pulmonary vein diameters and less flow disturbance. Additionally, the analysis showed that the LAA depth plays a crucial role in determining the thrombus formation potential, since it is directly related to effective blood washout. In general, shallower left atrium appendages presented a lower thrombogenic risk. The study highlighted the importance of a detailed hemodynamic analysis to assess thromboembolic risk in patients with atrial fibrillation, with particular emphasis on atrial anatomy and flow characteristics.

5. Acknowledgement

This study was financed in part by the Coordenação de Aperfeiçoamento de Pessoal de Nível Superior - Brasil (CAPES) - Finance Code 001. The authors would also like to thank the financial support provided by CNPq (National Council for Scientific and Technological Development, Process 405055/2023-4) and the scholarship program of the Federal University of ABC (UFABC).

6. Conflict of Interest

The authors declare do not have conflict of interest.

References

[1] E. J. Benjamin et al., "Heart disease and stroke statistics-2019 update: a report from the american heart association," Circulation, vol. 139, pp. e56–e528, 2019.

[2] M. García-Villalba et al., "Demonstration of patient-specific simulations to assess left atrial appendage thrombogenesis risk," Front. Physiol., vol. 12, p. 596596, 2021.

[3] W. P. Wodchis et al., "A review of the cost of atrial fibrillation," Value Health, vol. 15, no. 2, pp. 240–248, 2012.

[4] G. M. Bosi et al., "Computational fluid dynamic analysis of the left atrial appendage to predict thrombosis risk," Front. Cardiovasc. Med., vol. 5, p. 34, 2018.

[5] A. L. Olivares et al., "Combined analysis of virtual haemodynamics patterns and LAA morphologies in relation with the risk of thrombus formation," Eur. Heart J., vol. 38, p. 86, 2017.

[6] M. J. Mulder et al., "Left atrial appendage morphology in atrial fibrillation: do we prefer chicken wing or cauliflower?," J. Cardiovasc. Comput. Tomogr., vol. 14, no. 2, pp. 201–202, 2020.

[7] L. Wu et al., "Relation of left atrial appendage morphology determined by computed tomography to prior stroke or to increased risk of stroke in patients with atrial fibrillation," Am. J. Cardiol., vol. 123, pp. 1283–1286, 2019.

[8] R. Fang et al., "Impact of left atrial appendage location on risk of thrombus formation," Biomech. Model. Mechanobiol., vol. 20, no. 4, pp. 1431–1443, 2021.

[9] A. Masci et al., "The impact of left atrium appendage morphology on stroke risk assessment in atrial fibrillation: A computational fluid dynamics study," Front. Physiol., vol. 9, pp. 1–11, 2019.

[10] C. H. Roney, I. Sim, J. Yu et al., "Predicting atrial fibrillation recurrence by combining population data and virtual cohorts of patient-specific left atrial models," Circ. Arrhythm. Electrophysiol., vol. 15, no. 2, p. e010253, 2022.

[11] J. Lameu, I. Sandoval, and J. Salinet, "Thrombogenesis and hemodynamic in left atrium under atrial fibrilation," Comput. Cardiol., vol. 49, 2022.

[12] G. C. Fernández-Pérez et al., "Analysis of left ventricular diastolic function using magnetic," Radiología, vol. 4, no. 4, pp. 295–305, 2012.

[13] J. Mill, V. Agudelo, A. L. Olivares et al., "Sensitivity analysis of in silico fluid simulations to predict thrombus formation after left atrial appendage occlusion," Mathematics, vol. 9, no. 18, p. 2304, 2021.

[14] C. Albors, J. Mill, A. L. Olivares, X. Iriart, H. Cochet, and O. Camara, "Impact of occluder device configurations in in-silico left atrial hemodynamics for the analysis of device-related thrombus," PLoS Comput. Biol., vol. 20, no. 9, p. e1011546, Sep. 2024.

[15] J. Mill, V. Agudelo, C. H. Li, J. Noailly, X. Freixa, O. Camara, and D. Arzamendi, "Patient-specific flow simulation analysis to predict device-related thrombosis in left atrial appendage occluders," REC Interv. Cardiol., vol. 3, no. 4, pp. 278–285, 2021.

[16] Q. Gao, H. Lin, J. Qian, X. Liu, S. Cai, H. Li, H. Fan, and Z. Zheng, "A deep learning model for efficient end-to-end stratification of thrombotic risk in left atrial appendage," Eng. Appl. Artif. Intell., vol. 126, Part D, 2023.

[17] D. Schwartzman et al., "Characterization of left atrium and distal pulmonary vein morphology using multidimensional computed tomography," J. Am. Coll. Cardiol., vol. 41, no. 8, pp. 1349–1357, 2023.

[18] J. R. López-Mínguez et al., "Comparison of imaging techniques to assess appendage anatomy and measurements for left atrial appendage closure device selection," J. Inv. Cardiol., vol. 26, pp. 462–497, 2024.

[19] N. M. Al-Saady et al., "Left atrial appendage: structure, function, and role in thromboembolism," Heart, vol. 82, pp. 547–554, 1999.

[20] J. O. Taylor et al., "Development of a computational model for macroscopic predictions of device-induced thrombosis," Biomech. Model. Mechanobiol., vol. 15, pp. 1713–1731, 2016.

[21] G. García-Isla et al., "Sensitivity analysis of geometrical parameters to study haemodynamics and thrombus formation in the left atrial appendage," Int. J. Numer. Methods Biomed. Eng., vol. 34, pp. 1–14, 2018.

João Lameu da Silva Jr.
Federal University of ABC (UFABC)
Alameda da Universidade, s/n, São Bernardo do Campo, Brazil
joao.lameu@ufabc.edu.br